# Fine-Scale Structure of a VORTEX Squall Line

Wen-Chau Lee
National Center for Atmospheric Research[1]
Boulder CO, 80307 USA

## Abstract

The fine-scale structure of a VORTEX squall line is revealed by the NCAR ELDOAR airborne Doppler radar. The kinematic structure of a 60 km long segment is retrieved using a 3-D variational analysis technique that solves the 3-component of the velocities simultaneous. This approach enables the recovery of the storm structures in regions with elevation angles exceeding 45°. The reflectivity field is also corrected for attenuation that is significant for X-band radars sampling convective storms.

The segment of the squall line exhibits large along-the-line structural variations. The initially linear reflectivity pattern was distorted into a line-echo-wave-pattern (LEWP) by a mesocyclone circulation. This mechanism may be different from that produces 'bow eches' where two counter rotating vortices are often found. Damaging winds were reported near the apex of the LEWP where the mesocyclone is located. The intensity of the mesoscyclone reaches $10^{-2}s^{-1}$ but does not produce a tornado. Intense reflectivity factor pockets (exceeding 55 dBZ) are found between 11-15 km altitude, an indication of hail being lifted and suspended by strong updraft. Evaluating the vorticity equation and the retrieved pressure and buoyancy fields may be able to clarify these mechanisms in the future.

## 1. Introduction[1]

An intense squall line developed on 7 May 1995 in the Texas panhandle during VORTEX-95. This NS-oriented squall line formed SE of Amarillo, TX, moved eastward into Oklahoma. By 2100 UTC (all times are in UTC), this squall line was about 600 km long and 100 km wide and produced extensive hail (1-3 cm diameter) damages when it moved into SW Oklahoma. A section of the squall line appeared as a line-echo-wave-pattern (LEWP) ~2100 and produced downburst damage on the ground near Willow, Oklahoma.

The close relationship between damaging wind events and LEWP has been documented in Nolan (1959). While investigating an aircraft accident on landing, Fujita (1977) proposed that a rear inflow jet could produce the radar echo distortion and link the downburst event to the term 'bow echo'. Lee et al. (1992) demonstrated that the formation and intensification of a counter rotating vorticity couplet was associated with the distortion of an elongated echo into a bow shape. Recently, Weisman (1993) successfully simulated a long-lived bow echo event associated with a vorticity couplet ('book-end vortices') and a rear inflow jet. Although WSR-88Ds have observed LEWP and damaging wind events frequently, dual-Doppler observations on LEWP have been rare.

The purpose of this paper is to present preliminary analyses on the evolution and fine-scale structure of this squall line segment using primarily the dual-Doppler radar analyses from the NCAR ELDORA data. Emphasis is placed on documenting the evolution of the LEWP and the structural variations along the 2-D squall line.

## 2. Methodology

Both the NCAR Electra and NOAA P-3 flew ~60 km legs about 8-10 km east of this squall line at two different altitudes, 700 m and 3 km, respectively. ELDORA collected data from 2010 to 2200 (a total of 12 flight legs) with a data gap between 2055 to 2108. With additional data sources from the Amarillo WSR-88D and surface measurements from NSSL ground team, the evolution and fine scale structure of this squall line segment and its accompanied mesocyclone and LEWP were documented over a 90-minute period.

ELDORA's 300 m along track resolution is able to resolve features with a wavelength ~2 km. The Doppler radar data were corrected for the navigation and pointing angles biases (Testud et al. 1995) and edited in the NCAR SOLO package (Oye et al. 1995). The squall line moved eastward while the individual

[1]Corresponding author address: Wen-Chau Lee, NCAR Remote Sensing Facility, Boulder, CO 80307. Email: wenchau@ucar.edu. NCAR is sponsored by the National Science Foundation.

cells moved NE to NNE from 13-20 m/s. The cell motion in each flight leg was determined by tracking the reflectivity pattern from the P3 lower fuselage radar PPI scans. Then, the Doppler radar data were advected to compensate for the cell motion and the difference in sampling time. The Doppler radar data were

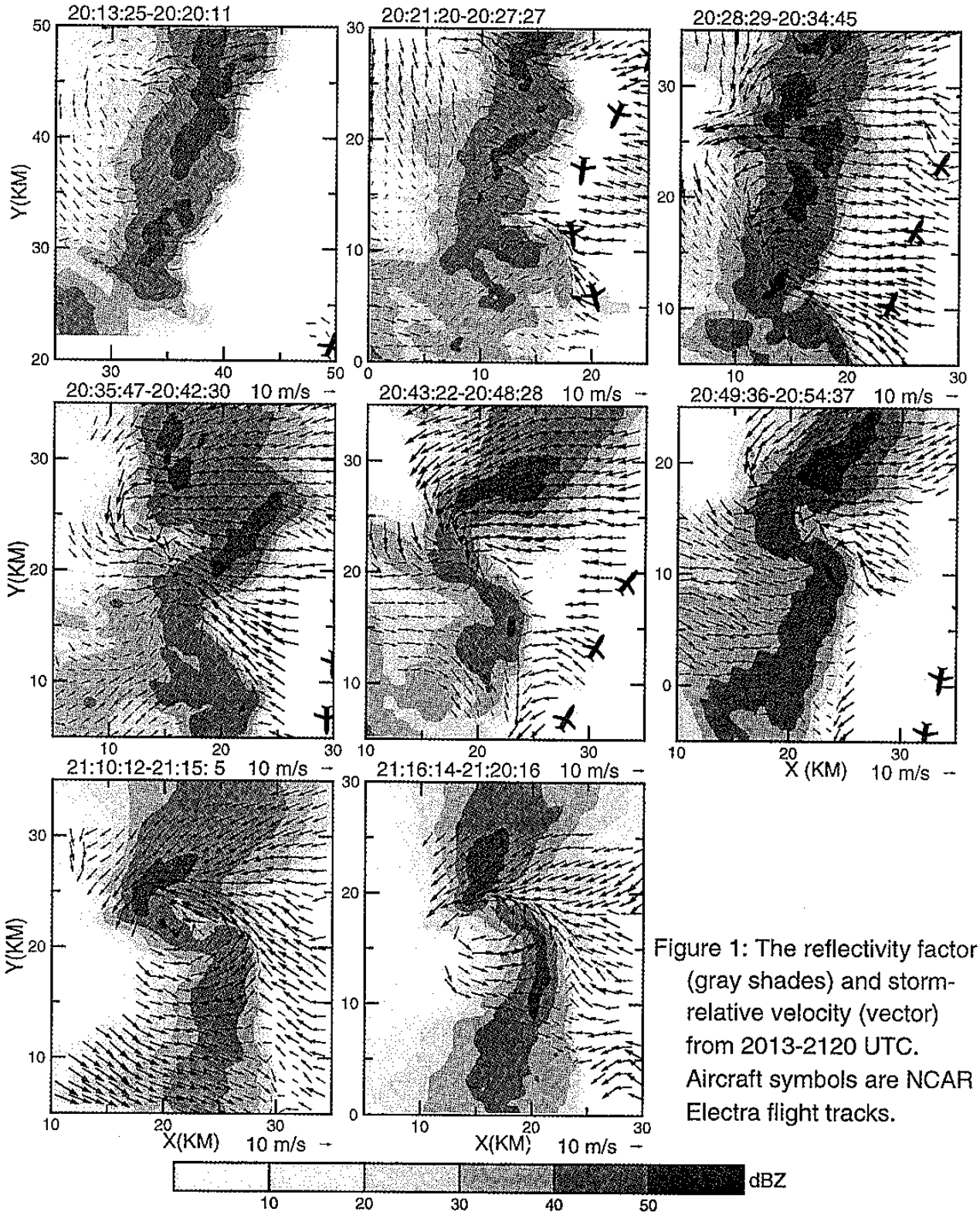


Figure 1: The reflectivity factor (gray shades) and storm-relative velocity (vector) from 2013-2120 UTC. Aircraft symbols are NCAR Electra flight tracks.

interpolated using Barnes scheme with grid spacing of 400 m in all three dimensions. The wind fields are deduced using a 3-D variational Doppler analysis technique (Gamache 1997) that solves the two radial velocity equations, anelastic mass continuity equation, and a smoothing function simultaneously with w=0 on top and bottom boundaries. The radial velocity equations are implemented as weak constraints while the continuity equation is a strong constraint. In this framework, the 3-D circulation can be retrieved even in the upper half of the storm, including the anvil region, where the conventional dual-Doppler analysis encounters difficulties.

The X-band airborne Doppler radar is subject to severe attenuation while sampling intense storms. A common practice to partially compensate for the attenuation chooses the higher reflectivity from fore or aft radar affecting a grid point. However, the results are not satisfactory even in moderate convective storms during TOGA COARE (Oury et al. 1999). Since Doppler velocity is lesser affected by attenuation than the reflectivity, the discrepancy in reflectivity field creates inconsistency in the retrieved kinematic and precipitation fields. The effect of attenuation is a more serious problem in mid-latitude convective storms where reflectivity exceeding 55 dBZ from intense precipitation and hail are quite common. In this study, the reflectivity factors are corrected using the method proposed in Oury et al. (2000) and will be shown side by side with the uncorrected reflectivity factors.

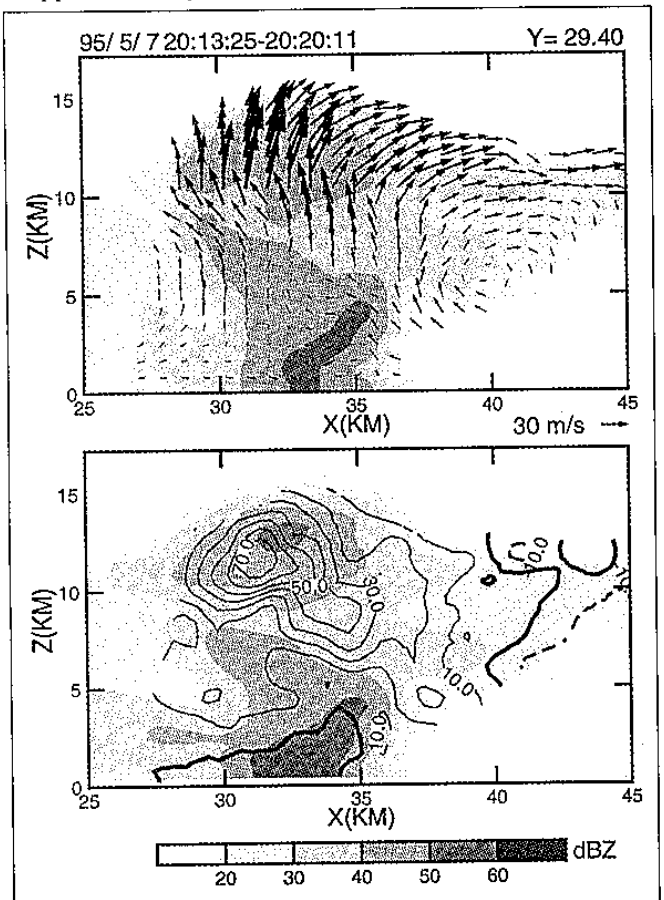


Figure 2: East-west vertical X-section at Y=29.4 km and 2013 UTC. Top panel shows the original reflectivity and velocity vectors. Bottom panel shows the attenuation corrected reflectivity and vertical velocity contours. Solid (dashed) lines represent updraft (downdraft).

### 3. Evolution of the mesocyclone and the LEWP

The horizontal reflectivity and storm-relative velocity fields for the first 8 flight legs at 2 km altitude are illustrated in Fig. 1. There was a mesocyclone accompanied by a hook echo signature located at [(35, 27), all coordinates hereafter are in km] in Fig. 1a at the beginning of the first leg. On leg 2 (Fig. 1b), Electra accidentally flew too close to the squall line and almost flew into the hook echo before it made a sharp turn. However, ELDORA collected a unique dataset beneath the vault (echo free region with intense updraft). Although the reflectivity pattern appeared linear in the NS direction, distinct low-level flow structures (e.g., Fig. 3b and c) on either side of the mesocyclone were

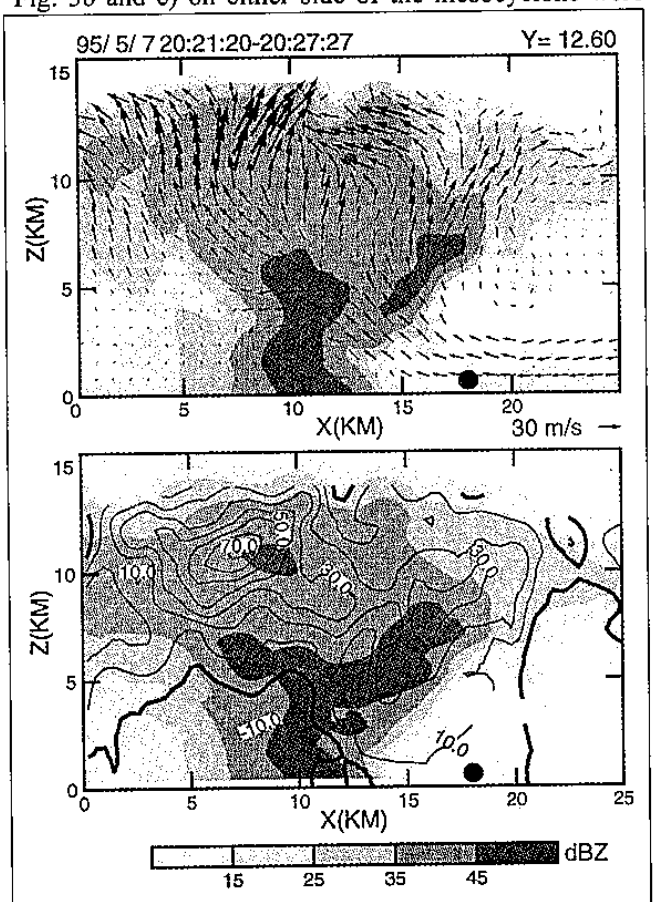


Figure 3: Same as Fig. 2 but for Y=12.6 km and 2021 UTC. Black dot is the aircraft.

clear. The convergence line between the environmental inflow and storm outflow was located near the eastern edge of the reflectivity gradient south of the mesocyclone while the convergence line bent near the mesocyclone and was located behind the reflectivity maximum north of the mesocyclone. This illustrates the 3-D nature of a squall line which is different from the conventional understanding on velocity convergence occurring at the leading edge of the line. In fact, the high reflectivity region north of the mesocyclone was the precipitation produced by the updraft south of the mesocyclone and was carried by the upper level SSW flow, then fell on the north side of the mesocyclone.

The mesocyclone reduced to a shear line in leg 4 (Fig. 1d) but reappeared in leg5 (Fig. 1e). The echo kink [(18,17) in Fig. 3d] was associated with a strong inflow jet. This inflow was consistent with the further destortion of the reflectivity pattern. In the mean time, the westerly south of the mesocyclone pushed the southern part of the line eastward and formed a LEWP (e.g., Fig. 1e). At 2049 (Fig. 1f), the mesocyclone (~3 km diameter) was located at the apex of the LEWP with its vorticity exceeding $10^{-2}s^{-1}$ but no tornado was observed. This apex moved through Willow OK ~2100. Damage survey indicated that most of the damages near Willow were produced by strong southerly winds. This is consistent with the SSW ground-relative winds near the apex of the LEWP (not shown) by superimposing a 20 m/s NNE translation speed of the mesocyclone on top of the ~30 m/s mesocyclone winds.

After ELDORA was recovered at 2110 (Fig. 1g), a mesocyclone of ~10 km diameter was identified near the rear apex of the LEWP. The sharp convergence on the southern part of the line still existed but the overall circulation resembled a mesocyclone in 10-20 km scale.

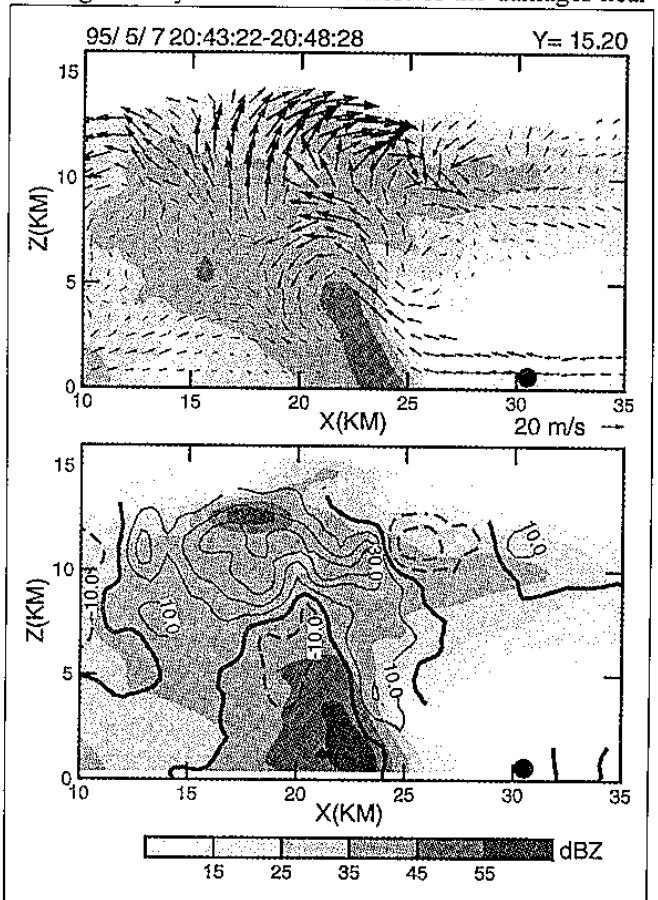


Figure 4: Same as Fig. 2 but for Y=15.2 km and 2043 UTC. Black dot is the aircraft.

#### 4. Vertical structures

The mesocyclone was always associated with strong updrafts. The E-W X-section across the mesoscyclone at 2013 (Fig. 2) showed an updraft exceeding 70 m/s at 11 km altitude just below the attenuation corrected 59 dBZ echo at 13 km altitude (the original reflectivity is 47 dBZ). The attenuation corrected reflectivity factor revealed detailed structures that would not be seen in the original reflectivity. The 59 dBZ echo was likely associated with ~2 cm diameter hail inferred from Foot and Wade (1982), in agreement with the 2-3 cm diameter hailstone observed in the storm vicinity (from Storm Data). The fall speed of a 2

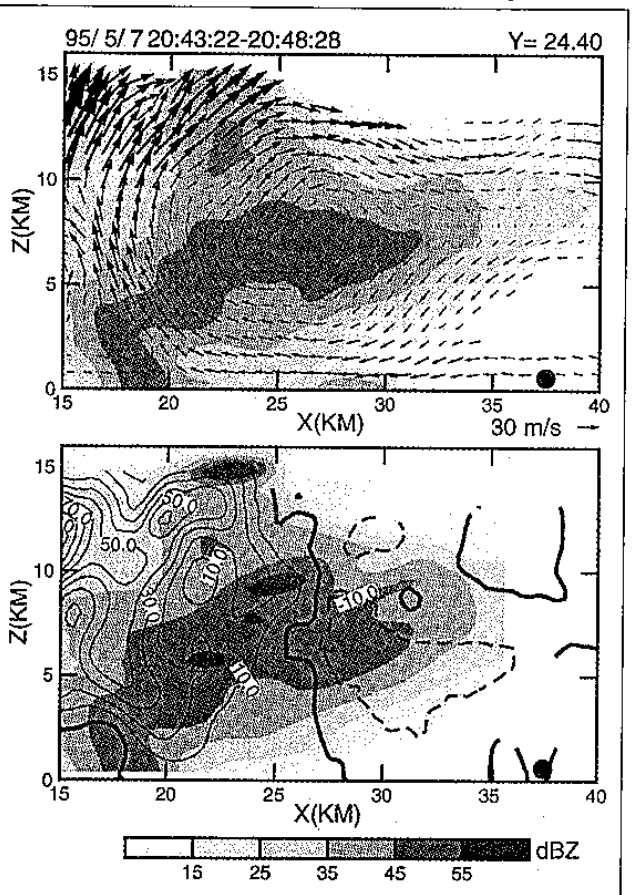


Figure 5: Same as Fig. 4 but for Y=24.4 km and 2043 UTC. Black dot is the aircraft.

cm diameter hailstone is ~45 m/s at 13 km altitude after the density corrections. Therefore, the retrieved 70 m/s plus vertical velocity, although unverified, seems plausible. The E-W X-section just north of the mesocyclone at 2021 (Fig. 3) shows a much more intense reflectivity structure (lower panel) at the leading edge of the storm. A deep layer of inflow (at least 2.5 km deep) fed into the storm. The vertical velocity in the vault region over the aircraft was ~30 m/s. Again, an echo exceeding 50 dBZ was retrieved at 10 km altitude associated with a 70 m/s updraft core. Coherent vertical velocity structures were consistent with the reflectivity structure near the storm top and over the aircraft (black dot). The rearward sloping interface between the environmental inflow and the outflow from the rear of the storm is clearly resolved that can be identified in the Doppler velocity field (not shown).

The different structures on either side of the mesocyclone can be illustrated in the vertical X-sections at 2043. On the south side of the mesocyclone (Fig. 4), the updraft was narrow near the leading edge of the squall line (x=25). The interface between the updraft (inflow) and downdraft (outflow) is ~60° from the horizontal (notice that the horizontal and vertical scales are the same). A horizontal vortex associated with the echo overhang centered at (26, 7) was also revealed. Part of the primary updraft reached the storm top but part of it fed into the downdraft in heavy precipitation. The characteristics in this X-section resembled the numerical simulations of a 2-D squall line by Fovell and Ogura (1988). The flow structure north of the mesocyclone showed somewhat different characteristics (Fig. 5). The updraft was much broader and the inflow (including the return branch of the outflow in the anvil) was much deeper than those shown in Fig. 4. However, the intensity of the updraft near the storm top was stronger in the northern part of the storm.

## 5. Summary and discussions

This study documents the kinematic structure of a segment of a long squall line that eventually evolved into a LEWP. The 3-D variational analysis technique and the attenuation corrections on the reflectivity field greatly improved the analysis beyond the capability of the conventional dual-Doppler analysis. Although the updraft magnitude appeared large in the upper part of the storm, its coherent structure with attenuation corrected reflectivity suggests that the overall circulation is plausible and the uncertainty in the vertical velocity is probably ~20%, comparable to the vertical velocity obtained in conventional method. Unfortunately, a more precise estimation of the vertical velocity uncertainty due to the unknown particle fall speed is not possible without insitu microphysical measurement.

The structures along the line were highly three-dimensional and the leading edge of the reflectivity gradient did not always represent the convergence line as current understanding. It is shown that the distortion of the reflectivity pattern into LEWP was by locally enhanced velocities associated with a mesocyclone and damaging winds occurred near the apex of the LEWP. The mechanism presented here may be somewhat different from that produced bow echoes where two counter rotating mesocyclones were usually found. Another interesting question is why this $10^{-2}s^{-1}$ mesocyclone did not produce a tornado? These questions will be studied via computation of the vorticity equation and dynamic retrievals.

**Acknowledgments:**

The authors thank Dr. John Gamache for providing the 3-D variational analysis program and Dr. Stephane Oury for providing the attenuation correction software.

**References:**

Foot, G. B., and C. G. Wade, 1982: The 22 July 1976 case study: Radar echo structure and evolution. *Hailstorms of the Central High Plains, Volume II: Case Studies of the National Hail Research Experiment.* Edited by Knight and Squires. 93-113.

Fovell, R. G., and Y. Ogura, 1988: Numerical simulation of a midlatitude squall line in two dimensions. *J. Atmos. Sci.*, **45,** 3846-3879.

Fujita, T. T., and H. R. Byers, 1977: Spearhead echo and downburst in the crash of an airliner. *Mon. Wea. Rev.*, **105,** 129-146.

Gamache, J. F., 1997: Evaluation of a fully three-dimensional variational Doppler analysis technique. Preprints, *28 th Conf. On Radar Meteorology*, 9-13 Sept. 1997, Austin, AMS.

Lee, W.-C., R. M. Wakimoto, and R. E. Carbone, 1992: The evolution and structure of a "bow-echo-microburst" event. Part II: The bow echo. *Mon. Wea. Rev.*, **120,** 2211-2225.

Nolan, R. H., 1959: A radar pattern associated with tornadoes. *Bull. Amer. Meteor. Soc.*, **40,** 277-279.

Oury, S., X. Dou, and J. Testud, 2000: Estimate of precipitation from the dual beam airborne radars in TOGA-COARE. Part II: Precipitation efficientcy in the 9th February 1993 MCS. . *J. Appl. Meteor.*, **39,** (In Press).

Oury, S., J. Testud, and V. Marecal, 1999: Estimate of precipitation from the dual beam airborne radars in TOGA-COARE. Part I: The K-Z relationships derived from Stereo- and Quad-beam analysis. *J. Appl. Meteor.*, **38,** 156-174.

Oye, R., C. Mueller, and S. Smith, 1995: Software for radar translation, visualization, editing and interpolation. Preprints, *27 th Conf. On Radar Meteorology*, 9-13 Sept. 1997, Vail, AMS, 359-363.

Testud, J., P. H. Hildebrand, and W.-C. Lee, 1995: A procedure to correct airborne Doppler radar data for navigation errors using the echo return from the earth surface. *J. Atmos. Ocean. Tech.*, **12,** 800-820.

Weisman, M. L., 1993: The genesis of severe, long-lived bow echoes. *J. Atmos. Sci.*, **50,** 645-670.